

A computational procedure for finding multiple solutions of convective heat transfer equations

S Mishra and T DebRoy

Department of Materials Science and Engineering, Pennsylvania State University,
University Park, PA 16802, USA

Received 29 March 2005, in final form 22 May 2005

Published 5 August 2005

Online at stacks.iop.org/JPhysD/38/2977

Abstract

In recent years numerical solutions of the convective heat transfer equations have provided significant insight into the complex materials processing operations. However, these computational methods suffer from two major shortcomings. First, these procedures are designed to calculate temperature fields and cooling rates as output and the unidirectional structure of these solutions preclude specification of these variables as input even when their desired values are known. Second, and more important, these procedures cannot determine multiple pathways or multiple sets of input variables to achieve a particular output from the convective heat transfer equations.

Here we propose a new method that overcomes the aforementioned shortcomings of the commonly used solutions of the convective heat transfer equations. The procedure combines the conventional numerical solution methods with a real number based genetic algorithm (GA) to achieve bi-directionality, i.e. the ability to calculate the required input variables to achieve a specific output such as temperature field or cooling rate. More important, the ability of the GA to find a population of solutions enables this procedure to search for and find multiple sets of input variables, all of which can lead to the desired specific output. The proposed computational procedure has been applied to convective heat transfer in a liquid layer locally heated on its free surface by an electric arc, where various sets of input variables are computed to achieve a specific fusion zone geometry defined by an equilibrium temperature. Good agreement is achieved between the model predictions and the independent experimental results, indicating significant promise for the application of this procedure in finding multiple solutions of convective heat transfer equations.

(Some figures in this article are in colour only in the electronic version)

1. Introduction

In recent decades, the numerical solutions of the Navier–Stokes equation and the energy equation have provided useful information about various complex materials processing operations. The computed temperature fields, cooling rates, the shape and the size of the fusion zone (FZ), solidification front velocity and the velocity fields in the molten region have provided significant insight into the materials processing operations and the nature of the processed products that could not have been obtained otherwise [1–27]. However, these

calculation procedures have not found extensive use because of several shortcomings.

First, the numerical solutions of the equations of conservation of mass, momentum and energy are designed to calculate the temperature and the velocity fields for a given set of input variables. For example, when a moving heat source interacts with a material, the input variables may include the radius of the heat source, total power, the distribution of the power and the relative motion between the heat source and the material [12, 17]. However, in many cases the desired temperature field or the cooling rate is known and the real

need is to determine the input variables that can produce the desired cooling rate or the temperature field. In other words, the reverse problem is sometimes more important than the forward problem and the unidirectional models cannot solve the reverse problem. Second and more important, the convective heat transfer problems are often highly non-linear and multiple solutions exist for many complex problems. For example, a given FZ geometry, defined by an equilibrium temperature surface, can result from multiple combinations of input variables. The current generation of numerical models cannot determine multiple pathways or multiple sets of input variables to achieve a particular output from the convective heat transfer equations.

Here we propose a new method that overcomes the aforementioned shortcomings of the commonly used solutions of the convective heat transfer equations. The ability of the genetic algorithm (GA) to find the global optimal solution independent of the initial guessed values [28–31] makes it appropriate for solving the reverse problem. In other words, the GA can calculate the required input variables to achieve a specific output such as temperature field or cooling rate. More important, the ability of the GA to find a population of solutions [28–31] enables the proposed procedure to search for and find multiple sets of input variables, all of which can lead to the desired specific output. Thus, the proposed computational procedure is capable of finding multiple solutions of convective heat transfer equations.

In the past, GA operations often involved binary coded strings to express variable values and the procedure was very intensive, computationally [29]. However, significant advances have been made in the application of GA in recent years. Recently developed real number based GAs have been shown to be highly efficient, computationally. In particular, parent centric, generalized, generation gap GA has been shown to provide rapid convergence [30, 31]. To demonstrate the capabilities of the proposed computational method, it has been applied to convective heat transfer in a liquid layer locally heated on its free surface by a heat source. The heat source, an electric arc, moves linearly on a steel plate and forms a liquid pool. The liquid steel undergoes strong recirculation driven mainly by a combination of electromagnetic and Marangoni forces and, to a much lesser extent, the buoyancy force. The velocity field within the molten metal pool and the temperature field in the entire steel plate, can be obtained by numerically solving the equations of conservation of mass, momentum and energy in three dimensions. The input variables include the arc current, voltage and the scanning speed. Unlike conventional convective heat transfer calculation procedures, the method proposed here can be used to determine multiple combinations of input variable sets, all of which can result in a target FZ geometry determined by an equilibrium temperature. In effect, this paper shows that the proposed computational procedure can be applied to find multiple sets of solutions, i.e. sets of input variables. Each set of input variables can result in a specified output such as the depth and the width of the molten pool. The multiple solutions are verified by comparing them with the independent experimental measurements.

2. Mathematical model

2.1. Modelling of heat transfer and fluid flow in the FZ

An incompressible, laminar and Newtonian liquid flow is assumed in the molten metal pool. The linear momentum conservation equation for the j th direction is given by [12, 17]

$$\rho \frac{\partial u_j}{\partial t} + \rho \frac{\partial(u_i u_j)}{\partial x_i} = \frac{\partial}{\partial x_i} \left(\mu \frac{\partial u_j}{\partial x_i} \right) + S_j, \quad (1)$$

where ρ is the density, t is the time, x_i is the distance along the $i = 1, 2$ and 3 directions, u_j is the velocity component along the j direction, μ is the viscosity and S_j is the source term for the j th momentum equation and is given as [12, 17]

$$S_j = -\frac{\partial p}{\partial x_j} + \frac{\partial}{\partial x_j} \left(\mu \frac{\partial u_j}{\partial x_j} \right) - C \left(\frac{(1 - f_L)^2}{f_L^3 + B} \right) u_j - \rho U \frac{\partial u_i}{\partial x_i} + S b_j, \quad (2)$$

where p is the pressure, f_L is the liquid fraction, B is a constant introduced to avoid division by zero, C ($=1.6 \times 10^4$) is a constant that takes into account solid–liquid mushy zone morphology, U is the scanning speed and $S b_j$ represents both the electromagnetic and the buoyancy source terms. The third term on the right-hand side of equation (2) represents the frictional dissipation in the mushy zone according to the Carman–Kozeny equation for flow through a porous media. The pressure field was obtained by solving the following continuity equation simultaneously with the momentum equation [12, 17]:

$$\frac{\partial(\rho u_i)}{\partial x_i} = 0. \quad (3)$$

The total enthalpy, H , is represented by a sum of sensible heat, h , and latent heat content, ΔH , i.e. $H = h + \Delta H$, where $h = \int C_p dT$, C_p is the specific heat, T is the temperature, $\Delta H = f_L L$, L is the latent heat of fusion, and the liquid fraction, f_L , is assumed to vary linearly with temperature in the solid–liquid mushy zone [12, 17]:

$$f_L = \begin{cases} 1, & T > T_L, \\ \frac{T - T_S}{T_L - T_S}, & T_S \leq T \leq T_L, \\ 0, & T < T_S, \end{cases} \quad (4)$$

where T_L and T_S are the liquidus and the solidus temperatures, respectively. The thermal energy transport in the steel plate can be expressed by the following modified energy equation [12, 17]:

$$\rho \frac{\partial h}{\partial t} + \rho \frac{\partial(u_i h)}{\partial x_i} = \frac{\partial}{\partial x_i} \left(\frac{k}{C_p} \frac{\partial h}{\partial x_i} \right) - \rho \frac{\partial \Delta H}{\partial t} - \rho \frac{\partial(u_i \Delta H)}{\partial x_i} - \rho U \frac{\partial h}{\partial x_i} - \rho U \frac{\partial \Delta H}{\partial x_i}, \quad (5)$$

where k is the thermal conductivity. Since the system is symmetrical about the vertical plane containing the locus of the arc, only half the steel plate is considered. The top surface of the molten pool is assumed to be flat for the sake of simplicity.

The velocity boundary condition is given by [12, 17]

$$\begin{aligned}\mu \frac{\partial u}{\partial z} &= f_L \frac{d\gamma}{dT} \frac{\partial T}{\partial x}, \\ \mu \frac{\partial v}{\partial z} &= f_L \frac{d\gamma}{dT} \frac{\partial T}{\partial y}, \\ w &= 0,\end{aligned}\quad (6)$$

where u , v and w are the velocity components along the x , y and z directions, respectively, and $d\gamma/dT$ is the temperature coefficient of surface tension. As shown in equation (6), the u and v velocities are determined from the Marangoni effect [12, 17]. The w velocity is zero since there is no flow of liquid metal perpendicular to the pool top surface. The heat flux at the top surface is given by [12, 17]

$$k \frac{\partial T}{\partial z} = \frac{dQ\eta}{\pi r_b^2} \exp\left(-\frac{d(x^2 + y^2)}{r_b^2}\right) - \sigma\epsilon(T^4 - T_a^4) - h_c(T - T_a), \quad (7)$$

where r_b is the arc radius of a circular region within which the arc power is focused, d is the dimensionless arc power distribution factor which determines the nature of distribution of the power density of the arc, Q is the total arc power, η is the arc efficiency, σ is the Stefan–Boltzmann constant, h_c is the heat transfer coefficient and T_a is the ambient temperature. The first term on the right-hand side of equation (7) is the heat input from the heat source, defined by a Gaussian heat distribution. The second and third terms represent the heat loss by radiation and convection, respectively. The boundary conditions are defined as zero flux across the symmetric surface (i.e. at $y = 0$) by [12, 17]

$$\frac{\partial u}{\partial y} = 0, \quad v = 0, \quad \frac{\partial w}{\partial y} = 0 \quad (8)$$

and

$$\frac{\partial h}{\partial y} = 0. \quad (9)$$

At all other surfaces, temperatures are taken as ambient temperature and the velocities are set to zero.

2.2. Method for the numerical calculation of heat transfer and fluid flow

In this study, the transient nature of the problem is transformed to steady-state mode by using a co-ordinate system that moves with the heat source [12, 17]. The governing equations of the conservation of mass, momentum and energy in three dimensions (3D) are discretized using the power law scheme [32]. The computational domain is divided into small rectangular control volumes. The discretized equations for the variables are formulated by integrating the corresponding governing equation over the control volumes. The detailed method of discretizing the governing equations is available in [12, 17]. The discretized equations are solved using the SIMPLE algorithm [32] to obtain the temperature and velocity fields. A $104 \times 66 \times 66$ grid system is used in the calculation and the corresponding computational domain has dimensions of 149 mm (length), 71 mm (width) and 60 mm (depth). Spatially non-uniform grids with finer grids near the heat source are used for the maximum resolution of variables.

Two conditions had to be independently satisfied for the convergence of each variable. First, the residuals for the

Table 1. Data used in the calculations [5].

Physical property	Value
Liquidus temperature, T_l (K)	1785.0
Solidus temperature, T_s (K)	1745.0
Density of metal, ρ (kg m^{-3})	7200.0
Thermal conductivity of solid, k_s ($\text{J m}^{-1} \text{s}^{-1} \text{K}^{-1}$)	25.08
Specific heat of solid, C_{ps} ($\text{J kg}^{-1} \text{K}^{-1}$)	702.24
Specific heat of liquid, C_{pl} ($\text{J kg}^{-1} \text{K}^{-1}$)	806.74
Temperature coefficient of surface tension, $d\gamma/dT$ ($\text{N m}^{-1} \text{K}^{-1}$)	-0.5×10^{-3}
Coefficient of thermal expansion, β (K^{-1})	1.5×10^{-6}
Viscosity of molten iron at 1823 K, μ ($\text{kg m}^{-1} \text{s}^{-1}$)	6.7×10^{-3}

Table 2. Input variables and experimentally measured depth and width of the FZ [5].

Arc current (A)	250.0
Arc voltage (V)	16.5
Scanning speed (mm s^{-1})	8.33
Depth of penetration (mm)	1.11
FZ width (mm)	5.17

velocities and the enthalpy had to be smaller than 10^{-4} . The residuals were defined as

$$\frac{\sum_{\text{domain}} |[\sum_{\text{nb}} a_{\text{nb}} \Phi_{\text{nb}} + S_U \Delta V]/a_P - \Phi_P|}{\sum_{\text{domain}} |\Phi_P|},$$

where a is the coefficient of the variable Φ in the discretized equation calculated based on the power law scheme [32], subscript P represents a given grid point, subscript nb represents the six neighbours of the given grid point P in the 3D orthogonal co-ordinate system, Φ is a general variable such as velocity or enthalpy, ΔV is the volume of the control volume and the coefficient a_P is defined as: $a_P = \sum_{\text{nb}} a_{\text{nb}} - S_P \Delta V$, where the terms S_U and S_P are used in the linearization of the source term, S , as: $S = S_U + S_P \phi_P$. Second, upon convergence, the ratio of (net heat input rate)/(total heat output rate + heat accumulation rate) should lie between 0.999 and 1.001 to satisfy the heat balance. More restrictive convergence conditions do not change the final results while increasing the computational time significantly.

The convective heat transfer calculations normally converge within 4000 iterations, which take about 5 min in a PC with 3.2 GHz Intel P4 CPU and 512 Mb PC2700 DDR-SDRAM memory.

The data used for the convective heat transfer calculations are given in table 1.

2.3. Genetic algorithm as an optimization model

A GA is used to search for multiple sets of important input variables, i.e. arc current, voltage and scanning speed, to achieve a target FZ geometry. This approach enables calculation of multiple pathways to achieve a target FZ geometry and provides a bi-directional capability to the proposed computational procedure. To start with, many initial sets of randomly chosen values of the three input variables are created. A systematic global search is next undertaken to find the optimum set of values of these input variables that leads to the least error between the calculated and the desired depth

and width of the FZ. The input variables and the measured FZ dimensions are given in table 2.

In order to calculate the multiple sets of input variables, the direct calculation of heat transfer and fluid flow must be undertaken many times with randomly chosen input variables, i.e. current, voltage and the scanning speed. The randomly chosen values of the three input variables do not always produce the desired FZ dimensions. The resulting mismatch between the computed and the desired FZ dimensions is expressed by the following objective function, $O(f)$:

$$O(f) = \left(\frac{p^c}{p^e} - 1\right)^2 + \left(\frac{w^c}{w^e} - 1\right)^2, \quad (10)$$

where p^c and w^c are the computed depth and width of the FZ, respectively, and p^e and w^e are the corresponding experimental values of the specified FZ geometry given in table 2. The objective function, $O(f)$, depends on the three input variables: current, I , voltage, V and scanning speed, U :

$$O(f) = O(f_1, f_2, f_3) = O\left(\frac{I}{I_r}, \frac{V}{V_r}, \frac{U}{U_r}\right), \quad (11)$$

where I_r , V_r and U_r are the reference values that represent the order of magnitude of the input variables. Note that equation (11) has been made non-dimensional in order to preserve the importance of all the three input variables by making their non-dimensional values comparable in magnitude. The GA produces new individuals, or sets of input variables, with iterations based on the evolutionary principles [30, 31]. The GA used in this study is a parent-centric recombination (PCX) operator-based generalized generation gap (G3) model [30, 31]. The specific application of this model for obtaining multiple sets of input variables to achieve the specified FZ geometry is described as follows. This model was chosen because it has a faster convergence rate on standard test functions when compared with other evolutionary algorithms [30, 31]. The algorithm for the model is as follows:

- (1) A population is a collection of many individuals and each individual represents a set of randomly chosen values of the three input variables, i.e. arc current, voltage and scanning speed. A parent refers to an individual in the current population. The best parent is the individual that has the best fitness, that is, it gives the minimum value of the objective function, defined by equation (10), in the entire population. The best parent and two other randomly selected parents are chosen from the population.
- (2) From the three chosen parents, two offsprings or new individuals are generated using a recombination scheme. PCX based G3 models are known to converge rapidly when three parents and two offsprings are selected [30, 31]. A recombination scheme is a process for creating new individuals from the parents.
- (3) Two new parents are randomly chosen from the current population.
- (4) A subpopulation of four individuals that includes the two randomly chosen parents in step 3 and two new offsprings generated in step 2 is formed.
- (5) The two best solutions, i.e. the solutions having the least values of the objective function, are chosen from the subpopulation of four members created in step 4. These two individuals replace the two parents randomly chosen in step 3.

- (6) The calculations are repeated from step 1 until convergence is achieved.

The above steps, as applied to this study, are shown in figure 1. The working of the model to find the input variables by minimizing the objective function is illustrated in figure 2. The recombination scheme (step 2) used in the present model is based on the PCX operator. A brief description of the PCX operator, as applied to the present problem of three input variables, is described as follows.

First, three parents, i.e. (f_1^0, f_2^0, f_3^0) , (f_1^1, f_2^1, f_3^1) , (f_1^2, f_2^2, f_3^2) are randomly selected from the current population. Here, the subscripts represent the three input variables, while the superscripts denote the parent identification number. The mean vector or centroid

$$\vec{g} = \left(\frac{f_1^0 + f_1^1 + f_1^2}{3}, \frac{f_2^0 + f_2^1 + f_2^2}{3}, \frac{f_3^0 + f_3^1 + f_3^2}{3}\right)$$

of the three chosen parents is computed. To create an offspring, one of the parents, say $\vec{x}^{(p)} = (f_1^p, f_2^p, f_3^p)$ is chosen randomly.

The direction vector, $\vec{d}^{(p)} = \vec{x}^{(p)} - \vec{g}$ is next calculated from the selected parent to the mean vector or centroid. Thereafter, from each of the other two parents, i.e. (f_1^1, f_2^1, f_3^1) and (f_1^2, f_2^2, f_3^2) , perpendicular distances, D_i , to the direction vector, $\vec{d}^{(p)}$, are computed and their average, \bar{D} , is found. Finally, the offspring, i.e. $\vec{y} = (f_1', f_2', f_3')$, is created as follows:

$$\vec{y} = \vec{x}^{(p)} + w_\zeta |\vec{d}^{(p)}| + \sum_{i=1, i \neq p}^3 w_\eta \bar{D} \vec{h}^{(i)}, \quad (12)$$

where $\vec{h}^{(i)}$ are the orthonormal bases that span the subspace perpendicular to $\vec{d}^{(p)}$, and w_ζ and w_η are randomly calculated zero-mean normally distributed variables. The values of the variables that characterize the offspring, $\vec{y} = (f_1', f_2', f_3')$, are calculated as follows:

$$f_1' = f_1^0 + f_{11} + f_{12}, \quad (13)$$

$$f_2' = f_2^0 + f_{21} + f_{22}, \quad (14)$$

$$f_3' = f_3^0 + f_{31} + f_{32}, \quad (15)$$

where

$$f_{11} = w_\zeta \left(\frac{2f_1^0 - f_1^1 - f_1^2}{3}\right), \quad (16)$$

$$f_{21} = w_\zeta \left(\frac{2f_2^0 - f_2^1 - f_2^2}{3}\right), \quad (17)$$

$$f_{31} = w_\zeta \left(\frac{2f_3^0 - f_3^1 - f_3^2}{3}\right), \quad (18)$$

$$f_{12} = w_\eta \left(\frac{a_2 + b_2}{2}\right) \left[1 - \left(\frac{2f_1^0 - f_1^1 - f_1^2}{3d}\right)^2\right], \quad (19)$$

$$f_{22} = w_\eta \left(\frac{a_2 + b_2}{2}\right) \left[1 - \left(\frac{2f_2^0 - f_2^1 - f_2^2}{3d}\right)^2\right], \quad (20)$$

$$f_{32} = w_\eta \left(\frac{a_2 + b_2}{2}\right) \left[1 - \left(\frac{2f_3^0 - f_3^1 - f_3^2}{3d}\right)^2\right]. \quad (21)$$

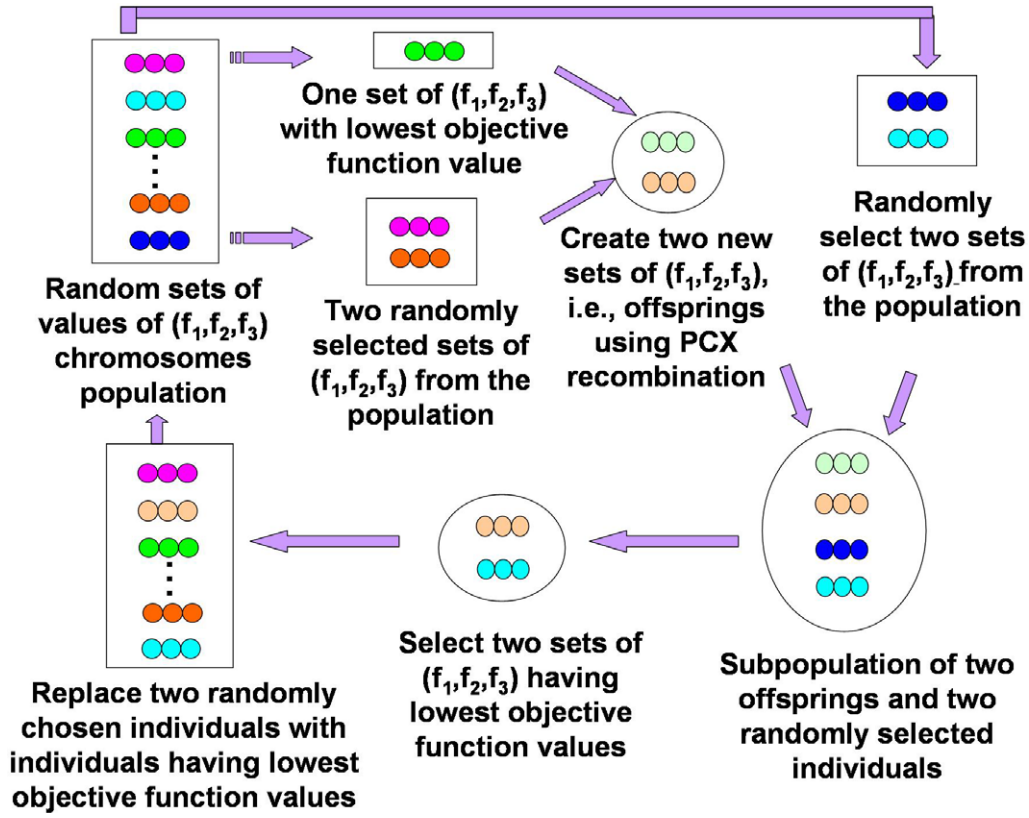


Figure 1. Generalized generation gap (G3) model using PCX operator.

The expressions for the variables d , a_2 and b_2 , used in equations (19)–(21), are as follows:

$$d = \left[\left(\frac{2f_1^0 - f_1^1 - f_1^2}{3} \right)^2 + \left(\frac{2f_2^0 - f_2^1 - f_2^2}{3} \right)^2 + \left(\frac{2f_3^0 - f_3^1 - f_3^2}{3} \right)^2 \right]^{1/2}, \quad (22)$$

$$a_2 = e_1 \times \sqrt{1 - (a_1)^2}, \quad (23)$$

$$b_2 = e_2 \times \sqrt{1 - (b_1)^2}, \quad (24)$$

where

$$a_1 = \sum_{i=1}^3 \frac{(f_i^1 - f_i^0)((2f_i^0 - f_i^1 - f_i^2)/3)}{d \times e_1}, \quad (25)$$

$$e_1 = \sqrt{(f_1^1 - f_1^0)^2 + (f_2^1 - f_2^0)^2 + (f_3^1 - f_3^0)^2}, \quad (26)$$

$$b_1 = \sum_{i=1}^3 \frac{(f_i^2 - f_i^0)((2f_i^0 - f_i^1 - f_i^2)/3)}{d \times e_2}, \quad (27)$$

$$e_2 = \sqrt{(f_1^2 - f_1^0)^2 + (f_2^2 - f_2^0)^2 + (f_3^2 - f_3^0)^2}. \quad (28)$$

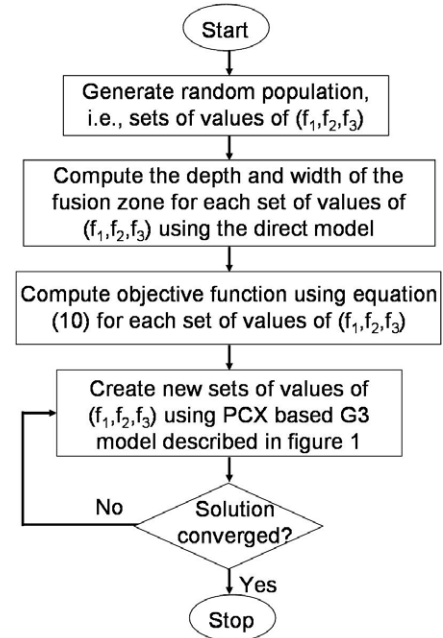


Figure 2. Flow chart of the G3 model.

3. Results and discussion

Three steps are involved in the calculation of the multiple sets of input variables to achieve a specified output or result from the convective heat transfer equations. First, a specified FZ geometry is identified by specifying the depth and width of the

FZ. Second the methodology described in this paper is utilized to calculate multiple sets of solutions, i.e. various combinations of arc current, voltage and scanning speed, with each solution capable of producing the same depth and width of the FZ. Third and finally, the results obtained from the model are adequately verified.

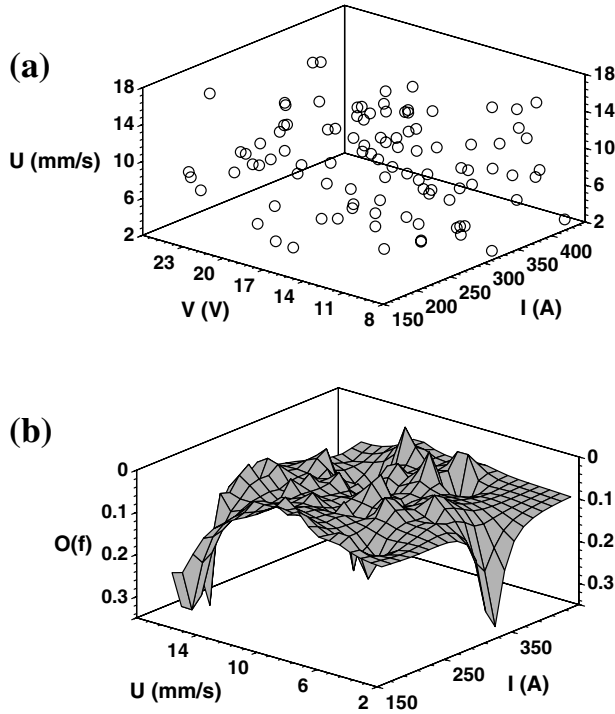


Figure 3. Initial population of randomly chosen values of input variable sets and their objective function values. (a) A large space of variables was searched to find optimum solutions as shown by the randomly selected initial input variable sets. (b) The low values of the objective functions of several individuals in the initial population indicate the possibility of existence of multiple optimal solutions.

As a first step, the depth and width of the FZ selected as an example are indicated in table 2. These values were experimentally obtained for a set of current, voltage and scanning speed indicated in the table. It is useful to specify these dimensions from an experiment because one of the solutions, i.e. the input variable set used to produce the FZ geometry is known. Thus, one of the solutions determined by the computational procedure must include the current, voltage and scanning speed combination used in the experiment. The other solutions must also be verified.

The second step, i.e. the calculation of the multiple solution sets starts by specifying a large random population of potential solutions, i.e. randomly generated sets of values of input variables of arc current, voltage and scanning speed. A population size of 100 input variable sets was used. This number of variable sets was determined based on how the population size influenced the effectiveness of GA using standard test functions [19, 30, 31]. Figure 3(a) depicts the initial values of the solutions, i.e. sets of current, voltage and scanning speed. The values of the input variables were chosen randomly within their appropriate ranges to maintain diversity in the input values and explore a large domain of input variables so as to include all possible solutions. The values of current were chosen in the range of 150–450 A, voltage in the range of 8–25 V and scanning speed in the range of 2–17 mm s⁻¹. The variable sets are then improved iteratively.

The progress of the iterative calculation is monitored by calculating the objective function values, defined by equation (10), for each set of input variables. A solution with

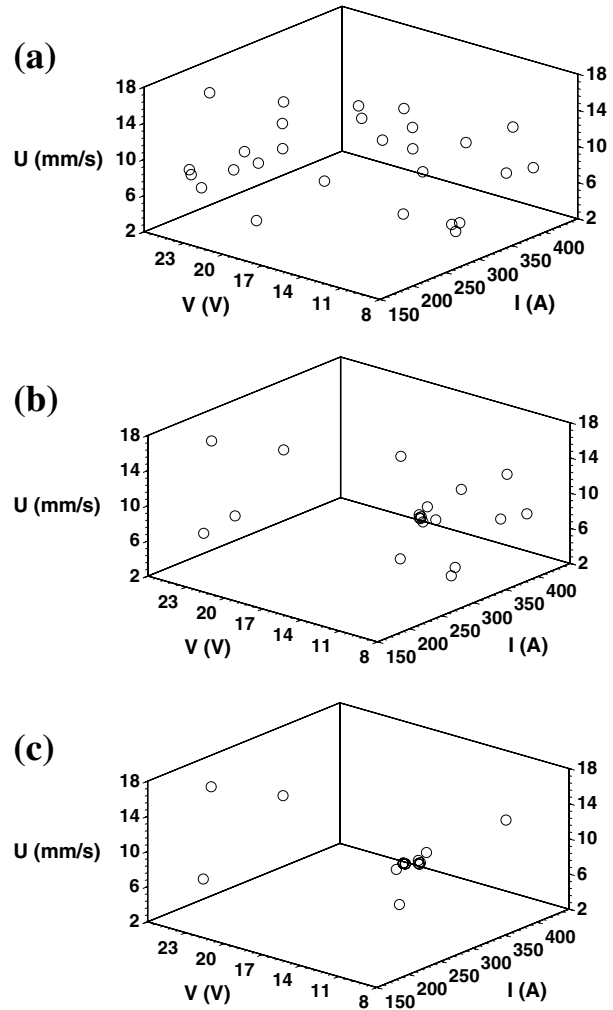


Figure 4. Several fairly diverse input variable sets could produce low values of the objective function indicating the existence of alternate paths to obtain the target FZ geometry. The plots show the input variable sets that produced low values of the objective function, $O(f)$ with iterations. (a) Individuals in the initial population with $O(f)$ less than 4.0×10^{-2} ; (b) individuals after five iterations with $O(f)$ less than 3.0×10^{-3} ; and (c) individuals after ten iterations with $O(f)$ less than 1.0×10^{-3} .

Table 3. Optimized sets of values of input parameters, i.e. arc current (I), arc voltage (V) and scanning velocity (U), to achieve the following target FZ dimensions: depth of penetration = 1.11 mm and width = 5.17 mm. The target FZ geometry was obtained experimentally using the following input variables: $I = 250$ A, $V = 16.5$ V and $U = 8.33$ mm s⁻¹.

Individual solutions	Current, I (A)	Voltage, V (V)	Scanning speed, U (mm s ⁻¹)
(a)	246.9	17.1	8.40
(b)	299.1	13.4	9.49
(c)	311.5	12.8	9.23
(d)	165.2	22.4	7.91
(e)	414.7	11.2	1.86
(f)	266.3	12.1	6.29

a low objective function value indicates that the set of input variable values it contains result in a small discrepancy between the computed and the specified FZ geometry. Figure 3(b) shows the computed values of the objective functions for

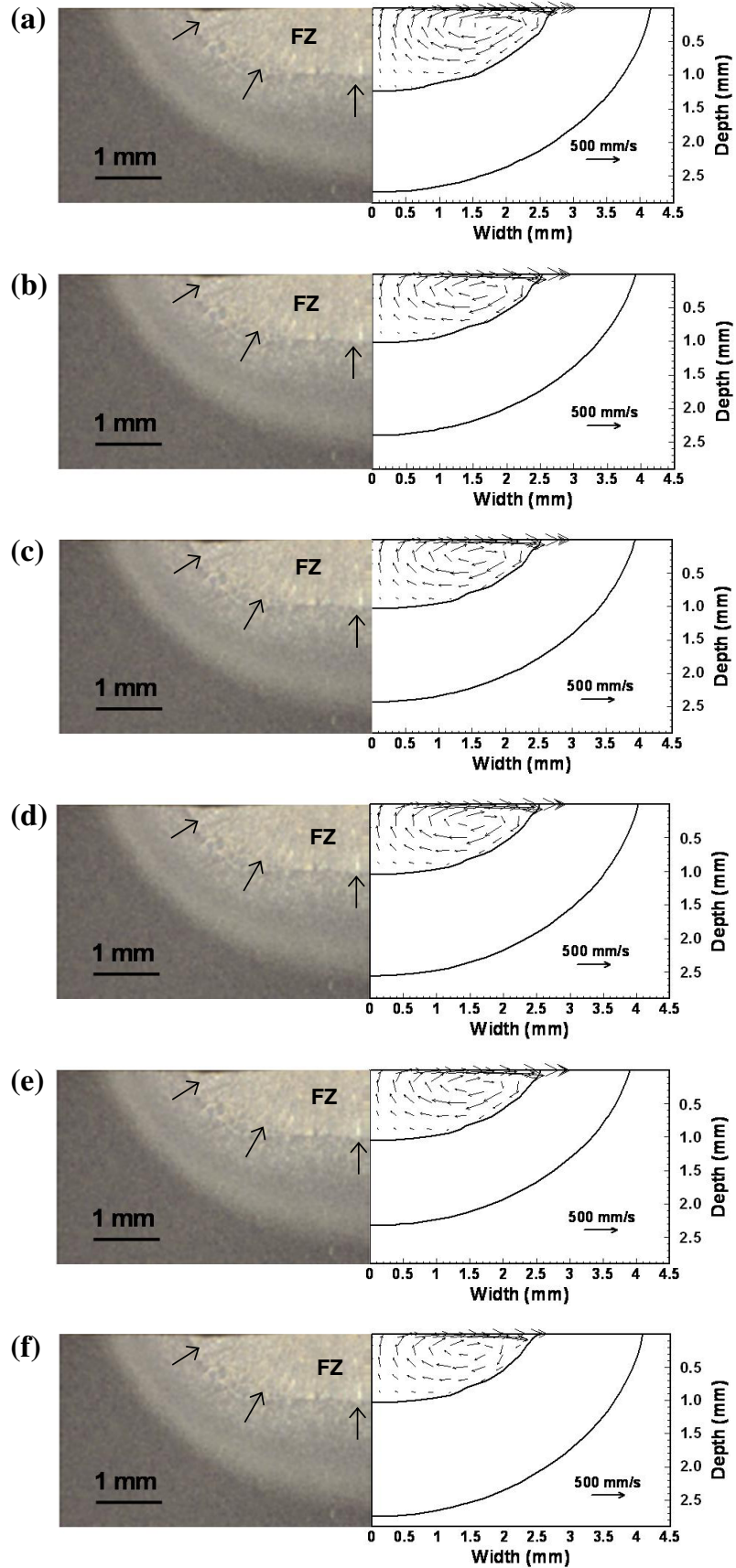


Figure 5. Comparisons between the calculated and the experimental FZ geometry for different optimized combinations of input variables given in table 3. The black arrows on the experimental micrograph indicate the location of the FZ boundary. The inner isotherm is 1745 K and represents the calculated FZ boundary. The outer isotherm is 773 K.

all the individuals depicted in figure 3(a). The plot shows that for many sets of input variables, the values of the objective function, $O(f)$, are fairly low, indicating that each of these input variable sets can produce a FZ geometry that is close to the specified geometry. Figures 4(a), (b) and (c) indicate several clusters of input variable combinations that have objective function values lower than 0.04, 0.003 and 0.001, corresponding to the 1st, 5th and 10th generation of individuals, respectively. It is noteworthy that in figure 4, the sets of input variables are distributed throughout the input variable space, signifying the existence of multiple paths to attain the specified FZ geometry. The progressive reduction of the objective function values of the best individuals indicates that the solutions are improved with generations (iterations). When the values of the objective function are low and do not decrease further with iterations, the computed input variable sets constitute the final solutions, which are presented in table 3.

Finally, the accuracy of the computed solutions was verified. For each individual solution listed in table 3, the depth and width of the FZ were calculated by using the forward convective heat transfer model and the computed values were compared with those obtained experimentally. Note that the values of current, voltage and scanning speed in solution (a) of table 3 are almost the same as the corresponding experimental values listed in table 2. The comparison between the computed and the experimental FZ dimensions is shown in figures 5(a)–(f). The FZ boundary on the experimental micrograph is indicated by black arrows. The calculated FZ boundary is marked by the solidus temperature of the steel, i.e. 1745 K. The calculated 773 K isotherm is also depicted in the figure, just to mark the area experiencing significant structural changes in the heat-affected zone (HAZ). The 773 K isotherm does not exactly depict the boundary of the HAZ. Figure 5 shows that the optimized input variable sets result in the correct prediction of the FZ shape and size in each case. The sets of values of the three input variables listed in table 3 are considerably different from each other. For example, the current values ranged from 165 to 414 A. The voltage ranged from 13.4 to 22.4 V and the scanning speed varied from 6.3 to 15.4 mm s⁻¹. All these differences in the important input variables indicate significant diversity in the paths, all of which lead to the same set of specified FZ dimensions. Thus, the proposed computational procedure, which combines the convective heat transfer calculations with a real number based GA, can find multiple pathways to achieve a specified FZ geometry.

4. Summary and conclusions

A computational method for finding multiple solutions of the convective heat transfer problem is proposed. The proposed methodology involves synthesis of a forward numerical procedure to solve the equations of conservation of mass, momentum and energy with a GA to overcome two important difficulties of the traditional solution procedures. First, the new methodology allows bi-directional capability so that it can be used to calculate the traditional input variables. Second, and more important, because of the highly non-linear nature of many convective heat transfer problems, multiple pathways

or solutions exist, with each solution capable of resulting in a specified output. The proposed methodology is capable of identifying multiple solutions through a global search for many solutions.

The methodology has been demonstrated in a convective heat transfer problem where a moving electric arc heats and melts a steel plate. A traditional unidirectional forward model that numerically solves the equations of conservation of mass, momentum and energy was combined with a real number based GA. The proposed methodology was used to calculate multiple combinations of arc current, voltage and scanning speed so that each combination was capable of resulting in a given depth and width of the FZ. The calculated solutions, i.e. combinations of current, voltage and scanning speed were tested by computing the FZ geometry from the temperature fields and comparing them with the specified depth and width of the FZ. Although the calculation procedure presented here focuses on the multiple sets of input variables that can each produce a given FZ geometry, similar calculations can easily be done for other specified attributes such as the cooling rates.

Acknowledgments

This research was supported by a grant from the US Department of Energy, Office of Basic Energy Sciences, Division of Materials Sciences, under grant number DE-FGO2-01ER45900. The authors thank Mrs Xiuli He, Mr Amit Kumar, Mr Rituraj Nandan and Mr Rohit Rai for their comments during the preparation of this paper.

References

- [1] Zhao H and DebRoy T 2003 *J. Appl. Phys.* **93** 10089
- [2] Zhang W, Kim C H and DebRoy T 2004 *J. Appl. Phys.* **95** 5210
- [3] Zhang W, Kim C H and DebRoy T 2004 *J. Appl. Phys.* **95** 5220
- [4] De A and DebRoy T 2004 *J. Appl. Phys.* **95** 5230
- [5] De A and DebRoy T 2004 *J. Phys. D: Appl. Phys.* **37** 140
- [6] Mishra S and DebRoy T 2004 *J. Phys. D: Appl. Phys.* **37** 2191
- [7] Mishra S and DebRoy T 2004 *Acta Mater.* **52** 1183
- [8] He X, Fuerschbach P W and DebRoy T 2003 *J. Appl. Phys.* **94** 6949
- [9] Kim C H, Zhang W and DebRoy T 2003 *J. Appl. Phys.* **94** 2667
- [10] Kumar A and DebRoy T 2003 *J. Appl. Phys.* **94** 1267
- [11] David S A, Trivedi R, Eshelman M E, Vitek J M, Babu S S, Hong T and DebRoy T 2003 *J. Appl. Phys.* **93** 4885
- [12] Zhang W, Roy G G, Elmer J W and DebRoy T 2003 *J. Appl. Phys.* **93** 3022
- [13] He X, Fuerschbach P W and DebRoy T 2003 *J. Phys. D: Appl. Phys.* **36** 3079
- [14] He X, Fuerschbach P W and DebRoy T 2003 *J. Phys. D: Appl. Phys.* **36** 1388
- [15] Elmer J W, Palmer T A, Zhang W, Wood B and DebRoy T 2003 *Acta Mater.* **51** 3333
- [16] Hong T and DebRoy T 2003 *Metall. Mater. Trans. B* **34** 267
- [17] Mundra K, DebRoy T and Kelkar K 1996 *Numer. Heat Transfer A* **29** 115
- [18] Kumar A and DebRoy T 2004 *Int. J. Heat Mass Transfer* **47** 5793
- [19] Kumar A, Mishra S, Elmer J W and DebRoy T 2005 *Metall. Mater. Trans. A* **36** 15
- [20] Lu S P, Fujii H and Nogi K 2005 *ISIJ Int.* **45** 66
- [21] Hong K, Weckman D C, Strong A B and Zheng W 2003 *Sci. Technol. Weld. Joining* **8** 313
- [22] Lu S P, Fujii H and Nogi K 2004 *Scr. Mater.* **51** 271

-
- [23] Fan H G and Kovacevic R 2004 *J. Phys. D: Appl. Phys.* **37** 2531
- [24] Suresh M V, Krishna B V, Venugopal P and Rao K P 2004 *Sci. Technol. Weld. Joining* **9** 362
- [25] Cao Z, Yang Z and Chen X L 2004 *Weld. J.* **83** 169s
- [26] Jaidi J and Dutta P 2004 *Sci. Technol. Weld. Joining* **9** 407
- [27] Ye X H and Chen X 2002 *J. Phys. D: Appl. Phys.* **35** 1049
- [28] Goldberg D E 1989 *Genetic Algorithm in Search, Optimization and Machine Learning* (Reading, MA: Addison-Wesley)
- [29] Back T, Fogel D B and Michalewicz Z (ed) 2000 *Handbook of Evolutionary Computation* (New York: Oxford University Press; Bristol: Institute of Physics Publishing)
- [30] Deb K, Anand A and Joshi D 2002 *Evol. Comput.* **10** 371
- [31] Deb K 2001 *Multi-Objective Optimization Using Evolutionary Algorithms* 1st edn (New York: Wiley)
- [32] Patankar S V 1980 *Numerical Heat Transfer and Fluid Flow* (New York: Hemisphere)